RESEARCH ARTICLE





Evaluation of commercial nanofiltration and reverse osmosis membrane filtration to remove per-and polyfluoroalkyl substances (PFAS): Effects of transmembrane pressures and water matrices

Qingquan Ma¹ | Qian Lei² | Fangzhou Liu¹ | Zimu Song¹ | Boris Khusid² | Wen Zhang^{1,2}

Correspondence

Wen Zhang, Department of Civil and Environmental Engineering, New Jersey Institute of Technology, Newark, NJ 07102, USA.

Email: wen.zhang@njit.edu

Funding information

National Science Foundation, Grant/Award Number: IIP 1822130

Abstract

Perfluoroalkyl and polyfluoroalkyl substances (PFASs) are now widely found in aquatic ecosystems, including sources of drinking water and portable water, due to their increasing prevalence. Among different PFAS treatment or separation technologies, nanofiltration (NF) and reverse osmosis (RO) both yield high rejection efficiencies (>95%) of diverse PFAS in water; however, both technologies are affected by many intrinsic and extrinsic factors. This study evaluated the rejection of PFAS of different carbon chain length (e.g., PFOA and PFBA) by two commercial RO and NF membranes under different operational conditions (e.g., applied pressure and initial PFAS concentration) and feed solution matrixes, such as pH (4-10), salinity (0- to 1000-mM NaCl), and organic matters (0-10 mM). We further performed principal component analysis (PCA) to demonstrate the interrelationships of molecular weight (213-499 g·mol⁻¹), membrane characteristics (RO or NF), feed water matrices, and operational conditions on PFAS rejection. Our results confirmed that size exclusion is a primary mechanism of PFAS rejection by RO and NF, as well as the fact that electrostatic interactions are important when PFAS molecules have sizes less than the NF membrane pores.

Practitioner Points

- Two commercial RO and NF membranes were both evaluated to remove 10 different PFAS.
- High transmembrane pressures facilitated permeate recovery and PFAS rejection by RO.
- Electrostatic repulsion and pore size exclusion are dominant rejection mechanisms for PFAS removal.
- pH, ionic strength, and organic matters affected PFAS rejection.
- Mechanisms of PFAS rejection with RO/NF membranes were explained by PCA analysis.

¹Department of Civil and Environmental Engineering, New Jersey Institute of Technology, Newark, New Jersey, USA ²Department of Chemical and Materials Engineering, New Jersey Institute of Technology, Newark, New Jersey, USA

INTRODUCTION

Perfluoroalkyl and polyfluoroalkyl substances (PFASs) have been increasingly detected in various environmental media—for example, air (D'Ambro et al., 2021), water (Rahman et al., 2014), and soil (Brusseau et al., 2020) due to their ubiquitous presence in industrial products. The third Unregulated Contaminant Monitoring Rule (UCMR 3) from the Environmental Protection Agency (EPA) requires to monitor six PFASs (i.e., PFOS, PFOA, PFNA, PFHxS, PFHpA, and PFBS) in drinking water systems (Hu et al., 2016). Removal of PFASs from water remains a daunting challenge due to the various properties (e.g., charges and structures) of PFASs and interferences from water matrices. Adsorption by powdered activated carbon (PAC) and granulated activated carbon (GAC) are proven effective for an extensive range of PFAS (Senevirathna et al., 2010; Zhi & Liu, 2015). Most of the studies indicate the removal of PFAS (4–6 carbons) reached 90%-99% through different GAC or PAC adsorption. However, adsorption of PFAS with small molecular weights, such as perfluorinated carboxylic acids (PFCAs) of <7 carbons and perfluorosulfonic acids (PFSAs) of <6 carbons, becomes less effective (Gagliano et al., 2020; Woodard et al., 2017; Zhang et al., 2019). For instance, nine commercial resins were tested to remove 40 PFAS at 600 ng·L⁻¹ from a drinking water source (Liu & Sun, 2021). The results indicate that the five polystyrenedivinylbenzene resins removed more than 90% of 35 PFAS compounds in 24 h, whereas polymethacrylate and polyacrylic resins only achieved >90% removal for up to 12 PFAS compounds. A pilot-scale GAC system operated over a 9-month period at a former military fire-fighter training site. For PFAS with equal perfluoroalkyl chain length, adsorbability for different head groups was in the order $-COO^- < -SO_3^- < -CH_2CH_2SO_3^- < -$ SO₂NH (Rodowa et al., 2020). However, both adsorption and ion exchange suffer high operational cost due to the backwashing required for regeneration. The disposal of the exhausted adsorbents and ion exchange resins is also costly (Cummings et al., 2015).

Membrane-based separation processes are widely applied in water treatment industries. Particularly, nanofiltration (NF) and reverse osmosis (RO) membranes are both effective for the rejection of 20 different PFAS (above 90%) with carbon chains of C1–C14 (Liu et al., 2022), including the two common ones, perfluor-ooctanoic acid (PFOA) and perfluorooctanesulfonic acid

(PFOS) (Bao et al., 2020; Boonya-Atichart et al., 2016, 2018; Chen et al., 2020; Das & Ronen, 2022; Espana et al., 2015; Franke et al., 2021; Gu et al., 2017; Lee et al., 2022; Liu et al., 2021, 2023; Mastropietro et al., 2021; Xiong et al., 2021; Yadav et al., 2022; Zhi et al., 2022). To reach high removal of PFAS in dilute matrixes such as source water for drinking water supply, NF/RO presents higher removal rates than GAC or ion exchange processes. Moreover, the replacement frequency for NF and RO membranes is much less than GAC (e.g., once every 6 months to 2 years) and ion exchange resin (e.g., every few months). Finally, NF and RO processes can employ a crossflow configuration to avoid the accumulation of solutes on the membrane surface and thus reduce the frequent system downtime to clean or replace the membrane elements. However, GAC and ion exchange resin often necessitate frequent backwashing and regeneration processes every 1 to 2 weeks or every 1-3 months, depending on the level of particulate loading. These procedures not only incur additional operational costs but also contribute to the overall waste generated, which tends to be less intensive for most NF/RO applications.

Full-scale NF and RO processes for the PFAS removal are demonstrated in Germany, Australia, Spain, and the US (Flores et al., 2013; Konradt et al., 2021; Liu et al., 2021). For instance, a parallel operation of two common technologies, low-pressure RO and activated carbon filtration, was investigated in a 5-month pilot study for the removal of 32 typical trace organic contaminants (including six different PFAS) from Rhine bank filtrates employing a semitechnical plant (Liu et al., 2023). NF membranes, owing to the negatively charged and hydrophilic surfaces, could strongly repel and reject those anionic PFAS with large molecular weight cut-off (MWCO). Rejection rates of >95% were reported for 15 PFASs (molecular weight: 263–713 g·mol⁻¹) utilizing four different NF membranes (NF270, NF200, DK, and DL) (Steinle-Darling & Reinhard, 2008). RO generally achieves higher PFASs rejection (>99%) than NF due to its denser active layer than the NF membranes (Baudequin et al., 2014). For example, a membrane with a MWCO of 500 Da will reject 90% of constituents with a molecular weight of 500 Da, such as PFOS. However, membrane filtration primarily relies on steric (size) exclusion, electrostatic repulsion, and other mechanisms (e.g., solute-diffusion or adsorption) to remove waterborne pollutants. Thus, PFASs such as perfluorobutane

sulfonic acid (PFBS) (338 Da) and perfluorooctanoic acid (PFOA) (414 Da) could pass through the NF membranes (Ross et al., 2018). Moreover, complex water chemistries such as pH, salinity, and the presence of organic matters could alter membrane surface properties (e.g., hydrophobicity and surface charge) as well as the acidic or anionic states of PFAS. Most of the findings suggest that the PFASs rejections by the membrane filtration partly depend on charge-driven exclusion, which is significantly affected by the solution pH. The higher the surface charge value, the better charge exclusion might be observed (Yadav et al., 2022). The ionic strength slightly affects the performance of RO and NF for the removal of PFASs. High ionic strength can shield the charge on the membrane surface and subsequently can reduce the rejection of PFASs, such as PFHxA (Franke et al., 2021). On the contrary, elevated ion strength could also enhance PFAS rejection by causing pore blockage and fostering specific bridging interactions with PFAS (Yadav et al., 2022). The organic matter, abundantly present in nature, can affect PFAS removal by interactions with PFAS and cause fouling on the membrane surface. So, the rejection of PFAS depends on the interactions among different PFAS in water and their further influence on the membrane surface (Chen et al., 2020; Zhi et al., 2022).

Recently, high-pressure (55 bar or higher) membrane filtration for RO or NF is gaining attention due to their increased water recovery (e.g., from 40%-60% to 95%) and reduced concentrate waste liquid for disposal. The operation of RO and NF under high pressures provided not only high-water recovery but also reduced some PFAS under the detection limits $(0.4-1.5 \text{ ng} \cdot \text{L}^{-1})$ in the treated effluent water (Das & Ronen, 2022). However, the micelle formation of PFAS on the membrane surface during the high-pressure filtration could reduce permeate flux and cause severe fouling or concentration polarization (CP). This surface accumulation of PFAS could also decrease the rejection by NF due to the reduced backdiffusion of PFASs through the fouling layer (Chen et al., 2020; Liu et al., 2023). Moreover, the membrane operational parameters, such as crossflow velocity, pH, temperature, and transmembrane pressure, significantly affect the membrane performance, such as permeate flux and pollutant rejection.

So far, there are still elusive understandings of the effects of the intrinsic (e.g., membrane and PFAS characteristics) and extrinsic factors (e.g., water matrices and filtration operations) on PFAS rejection by high-pressure RO/NF membrane filtration. Existing literature predominantly explored the influence of operating pressure, pH, Ca²⁺/Mg²⁺, humic acid (HA), and NF membrane properties on rejection performances for PFAS (Wang

et al., 2018). Moreover, most of the reported studies employed a single type of PFAS, either PFOA or PFOS, without examinations of shorter chained PFAS such as perfluorobutanoic acid (PFBA) and perfluorohexane sulfonate (PFHxS), which are often introduced in industrial product formulation (Wang et al., 2018). Besides PFAS functionality and membrane characteristics, feed water composition, such as pH, the presence of inorganic ions and organic matter, and operation conditions were also identified as important factors affecting PFAS rejection by high-pressure membranes. Still, a method to appropriately choose suitable NF or RO membranes for the removal of specific PFAS in water has not been established. This project aims to systematically investigate the rejection of a broad range of PFASs with different chain lengths or hydrophobicity (e.g., PFBA, PFpeA, PFHpA, PFOA, PFNA, PFDA, PFUnDA, PFBS, PFHxS, and PFOS) using commercial BW30-2540 RO and NF90-2540 NF membranes. Furthermore, this study also evaluated the PFAS rejection under different solution chemical variations such as pH, ionic strength, and organic matter contents as well as filtration conditions such as different transmembrane pressures and initial PFAS concentrations. To holistically assess these factors and interconnections on the rejection of PFAS via RO/NF membrane filtration, we conducted PCA using extensive literature data mining and streamlined the contributions and influence weights of the variables on PFAS rejection, which provides new insight into the development of functional membranes and rationale operational strategies for PFAS abatement.

METHODS AND MATERIALS

RO and NF membranes and characterization

Commercial BW30-2540 RO and NF90-2540 NF membrane elements were purchased from Dow FilmTec (Minneapolis, MN). These two membrane types were chosen due to their high rejection capability, durability, and standardized sizing for broad industrial applications. According to the manufacturer, both consist of an ultrathin polyamide barrier layer on the top surface, a microporous polysulfone intermediate layer, and a polyester support fabric. Table S1 summarizes the major membrane characteristics. The membrane elements were carefully disassembled to take out the RO or NF membrane sheet that were stored as dry coupons. All membranes were thoroughly rinsed with distilled (DI) water and soaked in a DI water bath for 24 h.

1554731, 2024, 2, Downloaded from https://onlinelbrary.wiley.com/do/10.1002/wer.10983 by Nj. institute of Technlogyg, Wiley Online Library on [2/05/2024]. Sethe Terms and Conditions (https://onlinelbrary.wiley.com/etrms-and-conditions) on Wiley Online Library for luces of use; OA articles are governed by the applicable Creative Commons Licenses

Membrane morphology was observed by a scanning electron microscopy (SEM, JEOL, JSM-7900F) with an energy dispersive X-ray (EDX) system. Cross-section samples were prepared by immersing a wetted membrane in liquid nitrogen for approximately 60 s and then pressing a razor blade against the back side of the membrane to fracture it. All samples were coated with gold/palladium (8.0 nm thickness) using a Cressington Sputter Coater 208 HR (Watford, UK) at a current of 40 mA. Fourier transform infrared spectroscopy (FTIR) was used to analyze surface chemical composition on a bench top FTIRspectrometer (Cary 670, Agilent Technologies, USA) using the Attenuated total reflectance (ATR) mode between 400 and 4000 cm⁻¹. Prior to atomic force microscopy (AFM) imaging, membrane samples were air dried and taped to a clean glass slide with double-sided tape. Membrane surface topography was then observed using a Bruker Dimension Icon AFM with a SCANASYST-AIR tip (2-nm tip radius, Bruker, MA). All images were flattened with a second-order flattening protocol and the average surface roughness (Ra) measured. For each sample, the average roughness of three scans at each of five random locations was used to determine the sample roughness. To evaluate the surface charge properties, the surface zeta potentials and isoelectric point (IEP) of the tested membranes are measured. The average pore size of the NF membrane was determined based on a pore transport model that incorporates steric (size) exclusion and hindered convection and diffusion from the rejection data of reference inert organic solutes (Nghiem et al., 2004), which is detailed in the Supporting Information.

Chemical and reagents

Selection and quantification of PFAS

In this study, we have explored a larger number of PFAS, including PFBA (C4), PFBS (C4), PFPeA (C5), PFHxS (C6), PFHpA (C7), PFOA (C8), PFOS (C8), PFNA (C9), PFDA (C10), and PFUnDA (C11), which contain different carbon chain length and different end charged groups (carboxylic and sulfonate groups) as shown in Table S2. All PFAS molecules were obtained from Fisher Scientific (PA, USA). One long chain $(7 \le C \le 14)$ (PFOA, C8) and one short chain $(1 \le C \le 6)$ (PFBA, C4) were selected for the most predominant PFAS in this study. The critical micelle concentration (CMC) of PFOA was reported at around 25 mM (Shih & Wang, 2013). This study employed a PFOA concentration of 10 ppm (around 0.02 mM), where the hemi-micelles were unlikely to form **PFAS** during our experiment conditions. All

concentrations are measured by an Agilent Liquid Chromatography with tandem mass spectrometry (Agilent 6470 Triple Quadrupole LC/MS) with the EPA Methods 533 as mentioned in our previous paper (Ma et al., 2023). The method detection limits (MDLs) for all PFAS used in this study are all listed in Table S2.

Other chemicals

All other chemicals including sodium chloride (NaCl), sodium hydroxide (NaOH), hydrochloric acid (36.5% to 38.0%), bovine serum albumin (BSA), fluvic acid (FA), and humic acid (HA) were all purchased from Fisher Scientific (PA, USA) erythritol (\geq 99%), xylose (\geq 99%), and dextrose (\geq 99%) were purchased from Sigma-Aldrich (MO, USA).

Experiments setup

Figure S1 shows the laboratory setup of the membrane filtration assembly at NJIT. A sample solution in both branches was fed from a 1-L polypropylene tank. Each branch of setup included a laboratory crossflow RO unit (Crossflow Cell CF042, Sterlitech, Kent, WA, USA) with a flat membrane of 42 cm² active area $(3.625'' \times 1.800'')$, slot depth 0.09") that had a maximum operating pressure of 70 bar and temperature of 80°C. Two high performance liquid chromatography (HPLC) dual-head digital pump were used to pump the feed solution under a flow rate control (LabAlliance Prep 100, Scientific Systems, State College, PA, USA) equipped with a pressure monitoring unit and a built-in pulse damper to deliver low flow rates with less than 2% RSD pulsations. The feeding temperature was consistently maintained at $25.0 \pm 0.5^{\circ}$ C throughout the experiment. Two identical membranes were prepared using a punch and die set provided by Sterlitech and mounted in two RO units. Multiple computerized sensors were applied to continuously monitor the feed temperature (Type J Transmitter, Cole Parmer 94770-02), operation pressure (Gauge Transmitter, Cole Parmer 68073-14) and pH (pH Transmitter, Cole Parmer 56717-20). As the HPLC pump maintained a constant flow rate, once the flow stabilized, the transmembrane pressure, read by the pressure gauge as shown in Figure S1, could reach a desired value by adjusting the ultra-precision needle valve (up to 200 bar, McMaster Carr, Robbinsville, NJ, USA) at the downstream of the RO units. The retentate and permeate from the process were recycled back to the feed tank. To ensure accurate results and eliminate the effects of membrane compaction, the membranes were pre-compacted by filtering

on Wiley Online Library for rules of use; OA articles are governed by the applicable Creative Commons License

-water^{__ 5}

Milli-Q water through them for at least 24 h until a steady-state flux was observed.

Membrane water permeability was evaluated using DI water at the same feed flow rate of 30 mL·min⁻¹ under 25°C, and transmembrane pressures of 13.79–55.16 bar for RO and 13.79 bar for NF membrane, which is defined by Equation (1) and equals to the retentate pressure as measured in our system. Permeate flux was measured gravimetrically by collecting and monitoring the feedwater at specified time intervals.

$$TMP = \frac{P_f + P_r}{2} - P_p \tag{1}$$

where P_f , P_r , and P_p are the pressures at feed inlet, retentate outlet, and permeate side. In our system, P_f is almost the same as P_r , while P_p can be considered as zero.

PFAS rejection and adsorption assessment

A series of membrane rejection experiments were conducted to evaluate the rejection of PFAS by the RO or NF membranes. The operational conditions, including transmembrane pressure, feed pH, and PFAS types or concentrations, were adjusted accordingly. We selected a wide range of transmembrane pressure (e.g., 13.79–55.16 bar) to cover the typical operating pressures for RO and a fixed TMP 13.79 bar for NF membrane with a constant initial PFOA and PFBA concentrations (1000-10,-000 ppb) to evaluate the rejection efficiencies in DI water without adding any other water matrices. Permeate and feed samples were collected after the system was equilibrated for 1 h at each condition. Rejection performance or rejection ratio (R) of RO and NF membranes was determined by comparing the PFAS concentrations in the feed (C_f) and permeate (C_p) samples:

$$R = 1 - \frac{C_{\rm p}}{C_{\rm f}} \tag{2}$$

To investigate the impacts of the feed solution pH on the PFAS rejection, the feed solution pH was adjusted (e.g., 4–10) with NaOH or HCl. Similarly, we also prepared the feed PFAS solutions that were spiked with 10, 100, and 1000 mM of sodium chloride (NaCl) or 1, 5, and 10 mM of HA, FA, and BSA as the representative organic matter and protein and used as common model foulant in filtration studies (Ang & Elimelech, 2007). Therefore, to determine the efficacy of the selected RO and NF membranes for rejection of PFASs with different chain lengths, linear PFASs molecules consisting of perfluorinated backbones ranging from 4 to 11 carbons have

been tested. Especially, the rejection efficiency and water flux for PFAS molecules with molecular weights similar or smaller than the membrane nominal cut-off will be assessed to gain new insights on the chain length dependent rejection mechanisms.

Adsorption of PFAS to the RO and NF membranes and the subsequent impact on rejection were investigated as illustrated in Figure S1. First, the membranes were removed from the filtration module to allow the PFASspiked solution to circulate at 30 mL·min⁻¹ for over 2 days to assess the adsorption of PFAS to the membrane system components (e.g., pipes and valves) other than the membrane elements themselves. Second, the same adsorption experiment was performed by placing the RO or NF membranes (42 cm² each) into the membrane module to determine adsorption of PFASs to the membranes. In the absence of the RO or NF membranes, the PFAS concentration in the influent (Cin: 10 ppm) and the PFAS concentration in the effluent (C_{eff}) were measured respectively after circulation of the PFAS solution in the membrane module for 2 days. In the presence of the RO or NF membranes, the initial PFAS concentration in the influent (C_{in}) , the PFAS concentration in the retentate (C_{re}) , and PFAS concentration in the permeate (C_{per}) were also measured, respectively. The percentage of membrane adsorption (M_{membrane}) of PFOA or PFBA was calculated by the following equation:

The mass balance of PFAS without the membranes inserted into the module:

$$V \times 10 = V \times C_{\text{eff}} + M_{\text{system}} \tag{3}$$

The mass balance of PFAS after placing the membranes into the module:

$$V \times 10 = V \times C'_{\text{eff}} + M_{\text{ads}} (M_{\text{membrane}} + M_{\text{system}})$$
 (4)

The mass ratio or percentage of the membrane adsorbed PFAS over the total PFAS present in the system:

$$M_{\text{membrane}} = \frac{V \times C'_{\text{eff}} - V \times C_{\text{eff}}}{V \times 10}$$
 (5)

where V is the circulated PFAS solution volume.

Statistical analysis

The results are shown by mean values \pm standard deviation (SD) from three duplicate or replicate experiments. The differences in degradation performance

15\$47531, 2024, 2, Downloaded from https://onlinelibrary.wiley.com/doi/10.1002/wer.10983 by Nj Institute Of Technology, Wiley Online Library on [28/05/2024]. See the Terms and Conditions (https://onlinelibrary.wiley.com/erms

) on Wiley Online Library for rules of use; OA articles are governed by the applicable Creative Commons Licens

between groups were tested using one-way analysis of variance (ANOVA) and post hoc test with the least significant differences (LSD) with significant difference at p < 0.05.

To comprehensively understand the influences and interrelationships of the reported factors, including intrinsic properties of the treatment systems such as membrane properties (e.g., membrane pore sizes, surface zeta potential, and hydrophobicity), PFAS types (e.g., carbon chain length), and concentrations and extrinsic properties such as feed water chemistry and operation conditions, we collected employed literature data from over 30 journal publications for principal component analysis (PCA). The quoted data are primarily rejection of various PFAS in different water matrices under different optional conditions such as transmembrane pressure, initial concentration and pH values. To ensure that the data points had the same weight, all collected parameters were standardized to a Z score with a standard deviation of 1 and a mean value of 0. All statistical analysis and data plotting were performed using Excel and Origin version 2020b.

RESULTS AND DISCUSSIONS

RO and NF membrane characterization

Morphology and structural properties

The SEM and AFM images in Figure 1a,b reveal the typical cross-sectional structures for the commercial thin film composite polyamide RO and NF membranes, which are composed of three layers, a top dense polyamide layer responsible for selectivity, a microporous polysulfone layer, and a nonwoven fabric layer as support. The polysulfone layer is typically several tens to hundreds of micrometers thick, and the polyamide layer is usually less than $1 \,\mu m$ thick. The thickness of RO and NF membranes are 80 and 20 µm, respectively. In many cases, membrane thickness can have a significant influence on performance (Davenport et al., 2020). The thickness can affect the rate of filtration and the size of particles that can be retained. Thicker membranes may have a higher particle retention capacity, but they can also reduce the flow rate. The thickness of a membrane could also impact its permeability and selectivity. Thicker membranes may offer greater selectivity but at the cost of reduced permeability. Furthermore, Figure 1c-e compares the pristine and DI water filtered RO membranes and shows that the surface roughness of the RO membrane significantly reduced after the filtration experiment due to the compression at high operation pressures (55.16 bar). Similarly, NF experienced the same surface roughness changes upon a long operation time (24 h) under high-pressure filtration as compared in Figure 1d-f. We have measured the surface roughness of the pristine and DI water filtered RO and NF membranes as shown in Figure 1g-j. The membrane surface morphology as indicated by various roughness parameters such as average roughness and root means square (RMS) roughness was slightly changed after filtration. For example, the roughness (R_{RMS}) decreased from 74.8 and 74.4 to 66.9 and 64.6 nm, respectively, for the pristine RO/NF membrane and the RO/NF membrane after 24 h filtration with DI water. The membrane surface roughness decreased by ~13% after 24 h of filtration for both membranes, primarily due to membrane compaction under high operation pressures.

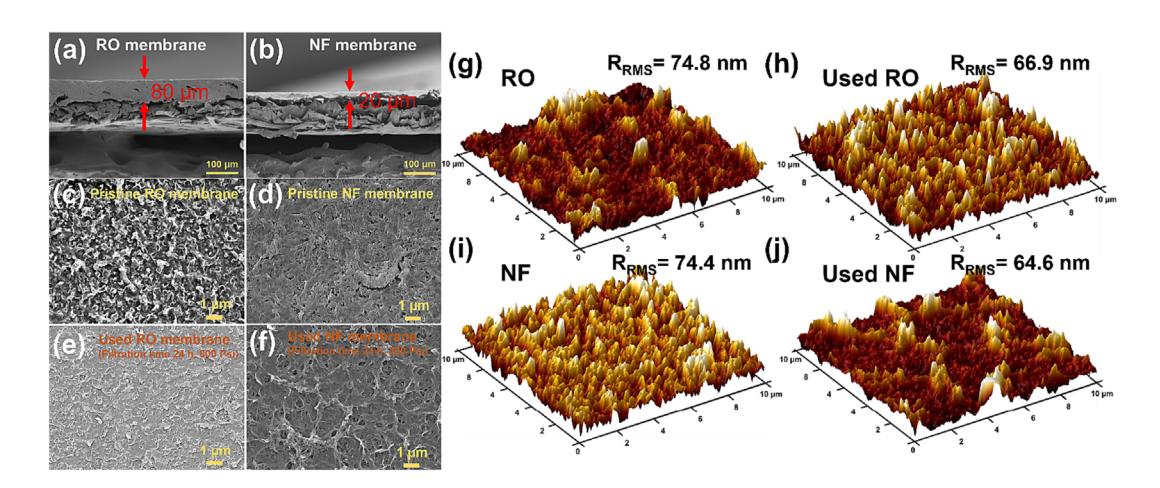
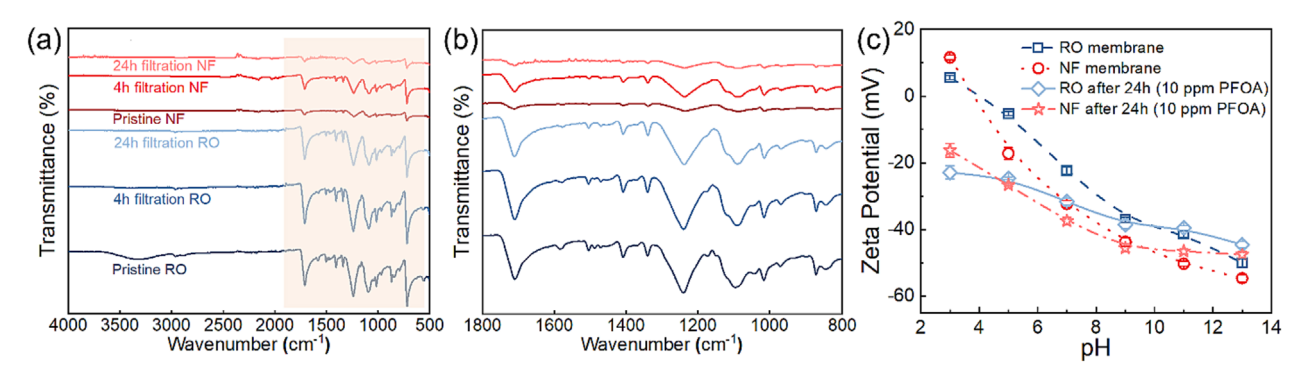


FIGURE 1 Scanning electron microscopy (SEM) of the (a,b) cross-section image of reverse osmosis (RO) and nanofiltration (NF) membrane; (c,d) pristine RO, NF membrane and (e,f) the distilled (DI) water filtered RO, NF membrane. Scale bar of 1 µm. AFM images of (g,h) pristine RO, NF membrane and (i,j) the DI water filtered RO, NF membrane.



(a,b) Attenuated total reflectance-Fourier transform infrared (ATR-FTIR) spectra of the reverse osmosis (RO) and nanofiltration (NF) membrane before and after perfluorooctanoic acid (PFOA) filtration. Experimental conditions: PFOA initial concentration of 10,000 ppb; feed flow rate of 30 mL·min⁻¹ room temperature; filtration time 4, and 24 h. (c) Surface zeta potential of RO and NF membrane before and after filtration.

Surface chemical properties

Figure 2a,b presents the ATR-FTIR spectra of the pristine and used RO and NF membranes after filtration experiments with PFOA. Compared with the spectra of pristine RO and NF membranes, the used membranes exhibited no characteristic peaks **PFOA** (e.g., stretching vibration of -CF_x at 1327 and 1106 cm⁻¹), suggesting the surface adsorption of PFOA on used RO or NF membranes was nondetectable by FTIR. The peaks at 1541, 1609, and 1641 cm⁻¹ in the FTIR spectra imply the characteristic functional groups in the polyamide layer of both RO and NF membranes that correspond to the amide II band related to N-H plane bending (Mouhoumed et al., 2014; Somrani et al., 2021). The peak at 1583 cm⁻¹ also suggests the existence of polyamide in BW30 membranes. The peaks located at 1145, 1180, 1235, 1280, 1350, 1385, 1488, and 1587 cm⁻¹ are attributed to the S=O stretching mode of polysulfone for both the pristine and the used BW30 and NF90 membranes (Mouhoumed et al., 2014). In terms of NF membranes, the presence of the peaks indicating characteristic Amide I (1680-1630 cm⁻¹) and Amide II (1570-1515 cm⁻¹) confirms that NF90 comprises an aromatic polyamide (Fernandez et al., 2011). For the enlarged ATR-FTIR spectra of RO and NF in the range 500-4000 cm⁻¹, the stretching vibrations at 3470 cm⁻¹ of both BW30 and NF90 exhibit N-H stretching band of amide groups that overlap with O-H stretching band (Mouhoumed et al., 2014). The changes in the FTIR spectrum of the NF membrane after 4 h can be attributed to chemical interactions or membrane structure changes. After 24 h, the membrane might have reached a state where the chemical interactions have stabilized or these structural changes might be reversible, leading to a spectrum that is somewhat

similar to the pristine membrane. Comparing the PFOA-adsorbed RO and NF membranes' spectra with that of the pristine membranes, the absence of obvious peaks formation or shifting in the spectrum suggests that the membrane surface may not exhibit significant changes at a macroscopic level. The confirmation of PFOA adsorption on the membrane surface may further require advanced techniques such as nanoscale infrared (nanoIR) spectrometers.

The surface zeta potentials of the RO and NF membranes were measured under different pHs at 25°C as shown in Figure 2c. The pristine RO and NF membranes were positively charged at low pH (<3) and mostly negatively charged at pH higher than pH = 3. The membrane surface zeta potentials were -22.3 ± 1.1 and -32.3± 1.3 mV for RO and NF membranes in DI water, respectively. The isoelectric points of both the RO and NF were 3.8 ± 0.5 and 4.3 ± 0.8 , respectively. The used RO/NF membranes after 24-h filtration with PFOA were more negatively charged over the tested pH range probably due to the surface adsorption of PFOA, though not detectable by FTIR.

Membrane permeability

Figure S2 shows that the permeate fluxes of the RO membrane at different applied transmembrane pressures, which shows a linear relationship and is in good agreement with results reported elsewhere (Tang et al., 2006). The water permeability coefficient (A) was determined to be $0.09 \pm 0.01 \text{ L} \cdot \text{m}^{-2} \cdot \text{h}^{-1} \cdot \text{psi}^{-1}$ by Equation (6): (Tang et al., 2006)

$$A = \frac{J_{\rm w}}{\Delta P} \tag{6}$$

1547531, 2024, 2, Downloaded from https://onlinelibrary.wiley.com/doi/10.1002/wer.10983 by Nj Institute Of Technology, Wiley Online Library on [28/05/2024]. See the Terms and Conditions

on Wiley Online Library for rules of use; OA articles are governed by the applicable Creative Commons Licenso

where J_w is the pure water flux (L·m⁻²·h⁻¹) and ΔP is the applied transmembrane pressure (bar). The water permeability coefficient of a membrane is generally constant unless the membrane is subjected to fouling or damage. The water permeability of NF membrane evaluated under operation pressure of 13.79 bar exhibited a stable permeate flux of 78.7 ± 0.8 L·m⁻²·h⁻¹, which corresponds to a membrane permeability of 0.4 L·m⁻²·h⁻¹·psi⁻¹.

Membrane pore size

We evaluated the average pore size of the pristine and used NF 90 membranes (1000 mM NaCl 24-h filtration under 13.79 bar). The real (intrinsic) retention of inert organic tracers (R_r) was obtained from the observed retention (R_o) by accounting for the effect of CP using Equation S3. The obtained real retentions were used to estimate the NF membrane average pore size using the membrane pore transport model described earlier. The estimated pore size is consistent for the different organic reference solutes as summarized in Table S3. On the basis of these results, we conclude that the pristine

NF 90 membrane has an average pore radius of 0.64 nm and used NF 90 membrane has an average pore radius of 0.78 nm, which is much larger than the pristine NF 90 membrane. The larger pore size of the used NF 90 membrane demonstrates that a high concentration NaCl during filtration will cause pore swelling with a relatively loose, nanoporous structure.

Effects of transmembrane pressure and initial concentration on PFAS rejection

Figure 3 presents the dependence of permeate flux and PFOA/PFBA rejection on the transmembrane pressure with the initial PFOA/PFBA concentration of 10,000 ppb, which was used to accelerate their penetration across the RO membrane and facilitate the instrumental detection. As shown in Table 1, both PFOA and PFBA concentration in permeate below the LC-QQQ detection limits when their initial feeding concentration was 1000 ppb, which thus does not allow us to assess the potency of PFAS rejection under different pressures. The permeate flux increased with the increase of the transmembrane pressure, due to the elevated driving force of the RO

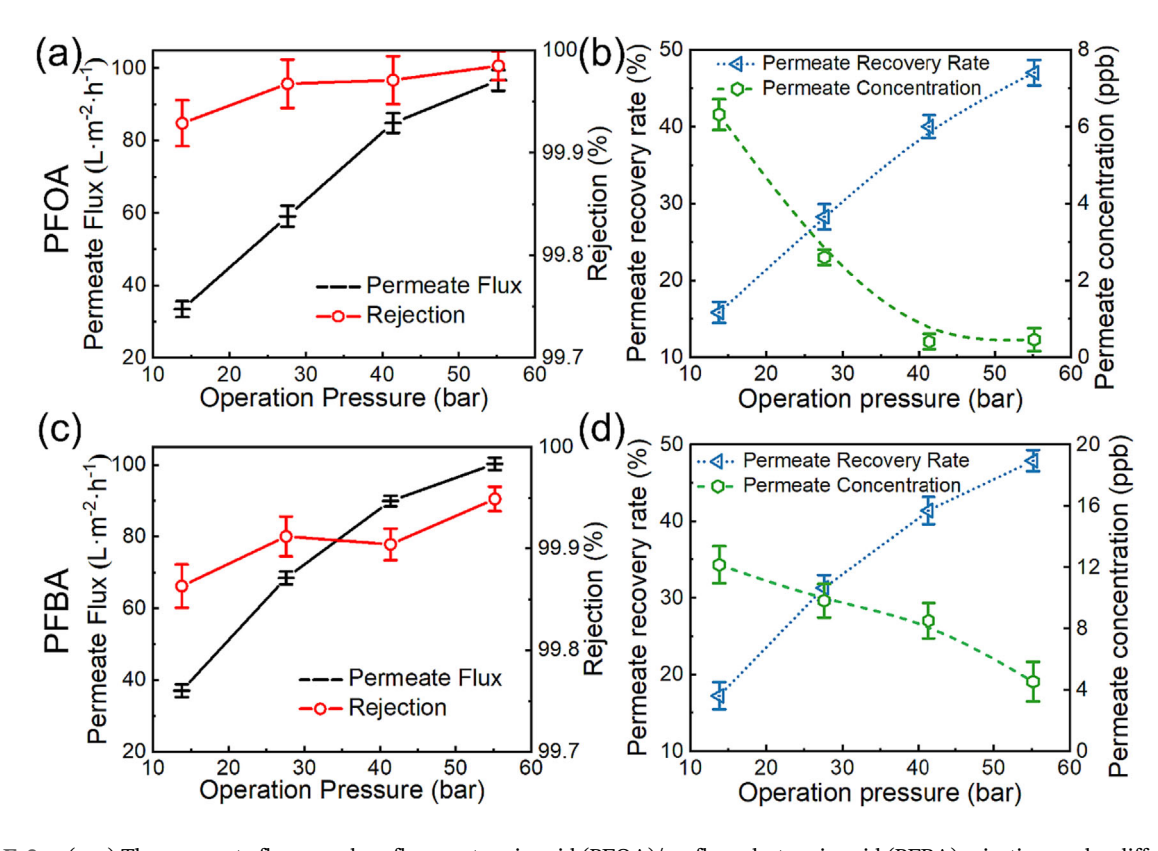


FIGURE 3 (a-c) The permeate fluxes and perfluorooctanoic acid (PFOA)/perfluorobutanoic acid (PFBA) rejection under different operation pressures on the reverse osmosis (RO) membrane. (b-d) The obtained permeate recovery rates and PFOA/PFBA concentrations in the permeate. Experimental conditions: PFOA/PFBA initial concentration of 10,000 ppb; feed flow rate of 30 mL·min $^{-1}$; room temperature; filtration time 24 h.

15547531, 2024, 2, Downloaded from https://onlinelibrary.wikey.com/doi/10.1002/wer.10983 by Nj Institute of Technology, Wiley Online Library on [28/05/2024]. See the Terms and Conditions (https://onlinelibrary.wikey.com/etrms-and-conditions) on Wiley Online Library for rules of use; OA articles are governed by the applicable Creative Commons Licenses

Effect of the initial PFCA concentration on the permeate flux and PFOA/PFBA rejection on the RO and NF membrane. Experimental conditions: a feed flow rate of 30 mL·min⁻¹ and a transmembrane pressure of 55.16 bar for RO and 13.79 bar for the NF membrane.

Membrane type	PFCA concentration (ppb)	Filtration time (h)	Permeate flux (LMH)	Permeate PFOA concentration (ppb)	Permeate PFBA concentration (ppb)
RO	1000	24	77 ± 0.4	0	0
	10,000	24	76 ± 3.9	5.20 ± 0.13	7.32 ± 0.24
NF	1000	24	78 ± 1.75	8.60 ± 2.74	12.61 ± 1.54
	10,000	24	79 ± 2.3	17.11 ± 3.39	27.16 ± 2.78

Abbreviations: NF, nanofiltration; PFBA, perfluorobutanoic acid; PFCA, perfluorinated carboxylic acid; PFOA, perfluoroctanoic acid; RO, reverse osmosis.

process. However, after the transmembrane pressure exceeded 40 bar, the permeate flux did not linearly increase as observed in Figure S2 for the DI water test, and instead the increase rate started to decline, due to the compression effect that may have reduced the pore size or water transfer channels. More importantly, when increasing the operation pressure, the PFOA/PFBA concentration in the permeate decreased and led to an increased PFOA/PFBA rejection. This could be attributed to the typical dilution effect of RO, wherein an increase in TMP results in an increase in water permeate flux and enhanced water recovery as shown in Figure 3b-d, while the solute PFAS flux is usually independent of the pressure and sterically hindered according to the classical solution-diffusion mechanism (Liu et al., 2021), leading to a higher solute or PFAS retention or rejection. The RO membrane has a well-defined pore size and molecular weight cut-off that will remain constant and thus yield a stable rejection performance even under increased pressures. In addition, the accumulation of PFAS on the membrane surface under high pressures may also hinder the further passage of PFAS under higher pressure, which resulted in lower PFAS concentration in the permeate as observed in Figure 3b-d and a higher PFAS rejection. For instance, Boontanon et al. reported that the rejection efficiency for PFOA by RO was slightly higher at elevated transmembrane pressure (>13 bar) (Boonya-Atichart et al., 2016). This is typically because the water flux is proportional to the TMP while the PFASs are independent of the pressure, which can be explained by the classical solution-diffusion mechanism.

Besides the PFAS rejection, the PFAS removal should consider the quantity of the PFAS in produced water or permeate, which was calculated by Equation (7).

Removal (%) =
$$\frac{QC_0 - Q'C_p}{QC_0}$$
 (7)

where Q is the feed flow rate (30 mL·min⁻¹), C_0 is the feed concentration (10,000 ppb), Q' is the permeate flow rate (mL·min⁻¹), and C_p is the permeate concentration (ppb). As the transmembrane pressure increased, the permeate flow increased proportionally with the reduced PFAS concentration in the permeate. Our calculation shows that above 99.98% PFOA or PFBA were removed by the RO membrane and the removal efficiency (%) also increased slightly as the transmembrane pressure increased from 13.79 to 55.16 bar as shown in Figure S4, suggesting that high-pressure RO operations could potentially increase both the permeate or water recovery and rejection or removal. High-pressure (e.g., 800 psi) RO processes are gaining high interests due to the potential for high yield and productivity. However, the removal efficiency and mechanisms of many potential micropollutants such as PFAS in such high-pressure RO processes are largely unknown, which is partially addressed in this study.

Table 1 also summarizes the PFCAs rejection by the NF membrane, which achieved 99.14% PFOA rejection and 98.32% PFBA rejection when initial concentration of PFCAs was 1000 ppb, the rejection of PFOA and PFBA decreased to 98.17% and 97.03% when initial concentration of PFCAs was 10,000 ppb, respectively. The main mechanisms for separating charged organic matter by NF membrane include electrostatic interaction, size exclusion, and adsorption. Because pKa values of PFOA and PFBA are very low, these target PFCAs would dissociate and be negatively charged at pH 7. Therefore, there was electrostatic repulsion between PFOA/PFBA and the negatively charged NF membrane, which benefitted rejection of target PFCAs. Moreover, the molecular weight and chain length of PFOA (413 g·mol⁻¹) are larger than the MWCO and pore size of NF membrane, respectively (Hang et al., 2015). However, the relation between PFBA and NF membrane was the opposite. Therefore, size

1554731, 2024, 2, Downloaded from https://onlinelbrary.wiely.com/do/10.1002/wer. 10983 by Nj. Institute of Technlogyg, Wiley Online Library on [208502024]. See the Terms and Conditions (https://onlinelbrary.wiely.com/terms-and-conditions) on Wiley Online Library on [208502024]. See the Terms and Conditions (https://onlinelbrary.wiely.com/terms-and-conditions) on Wiley Online Library for large for use; OA articles are governed by the applicable Creative Commons Licenses

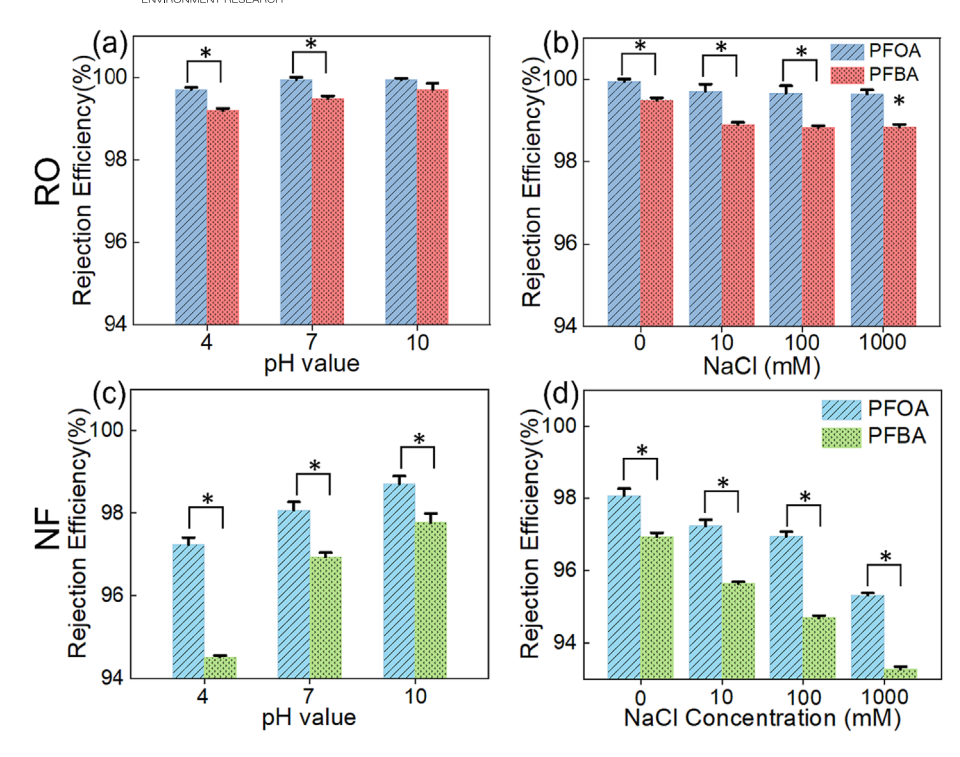


FIGURE 4 Rejection efficiencies of perfluorooctanoic acid (PFOA) and perfluorobutanoic acid (PFBA) by the reverse osmosis (RO) and nanofiltration (NF) membranes in different conditions. (a–c) Under different pHs; (b–d) under different NaCl concentrations. * represent significant differences (p < 0.05, t test) between PFOA and PFBA test group.

exclusion played an important role in PFOA rejection. In contrast, the effect of size exclusion on PFBA retention was weak.

The adsorption of PFAS on the RO/NF membranes or other membrane system components was first verified. Figure S3 shows that adsorption to both the membranes and membrane elements varied between 10% and 20% for different PFAS. The adsorption tends to be stronger for higher molecular weight PFAS. Additionally, adsorption of PFAS to the membranes and the membrane elements was similar and jointly may contribute to 20% or higher of the total removal rates. Thus, to make accurate calculations of the PFAS rejection rates, the remaining PFAS concentration in the rejected or recirculated feed solution have been corrected by considering this minor adsorption loss.

Effects of the feed solution pH, ionic strength, and organic matters on PFAS rejection

pH effect

As shown above in Figure 2c, pH could alter the surface charge of the membranes and the speciation of conjugate base and acid forms of PFAS. As shown in Table S2, at neutral pHs, most PFAS are anionic and should undergo electrostatic repulsion from the negatively charged RO or NF membranes. Figure 4a,c compares the PFOA and PFBA rejection on the RO and NF membranes when the

feed pH varied between 4 and 10. First, the rejection on RO did not exhibit high sensitivity to the pH variations as NF did, suggesting the PFAS rejection on RO is primarily attributed to the size exclusion, whereas the electrostatic repulsion is evident for PFAS on the NF membrane. Decreasing the feed pH from 10 to 4 consistently reduced the PFOA/PFBA rejection for both the RO and NF membranes, because both RO/NF membranes and PFOA/ PFBA became less negatively charged at low pHs and thus the PFAS-membrane repulsion decreased, which increases the likelihood of PFAS passage, especially for NF. One study employed four different NF membranes to filtrate 15 different PFAS with molecular weight ranging from 263 to 713 g·mol⁻¹ and found the 90% rejection cutoff point decreased from 500-550 g·mol⁻¹ to below 300 g⋅mol⁻¹ when pH increased from 2.8 to 5-6, suggesting an improved PFAS rejection at high pHs (Steinle-Darling & Reinhard, 2008). At low pHs, the membrane charge is neutral or positive; thus, the charge repulsion effect vanishes, resulting in a decrease in 90% rejection cutoff point. Soriano et al. reported that under the same neutral pH, the RO membrane with a higher negative charges or negative surface zeta potential rendered much higher rejection of PFHxA than those with the lower negative surface charges (Soriano et al., 2019).

Effect of ionic strength

Surface and ground water usually contain mineral ions such as calcium (Ca), magnesium (Mg), sodium (Na),



and potassium (K) (Banks et al., 2020), or typical anions such as nitrate or phosphate. PFAS and anions in water exhibit complex interactions with polymer membrane surfaces has been reported (Zhao et al., 2018). The electrostatic interactions can be enhanced by the increase of valence of the anions. For example, compared with the chloride (Cl⁻) and sulfate (SO₄²⁻), phosphate (PO₄³⁻) showed the most significant effect on the membrane rejection of PFOS, where phosphate seems to enhance electronegativity of the NF membrane surface after adsorption and thus increase the PFOA rejection (Luo et al., 2016). For cations or metal ions, such as Mg²⁺, Ca²⁺, and Fe³⁺, their presence was shown to increase the rejection rates of PFOS on commercial NF membrane (ESNA1-K1) membrane by 2%-3% (Zhao et al., 2018). Metal cations are believed to interact with the head functional groups of PFOS via electrostatic interactions, which increases the effective molecular size of PFAS and thus enables higher rejection by RO or NF (Luo et al., 2016).

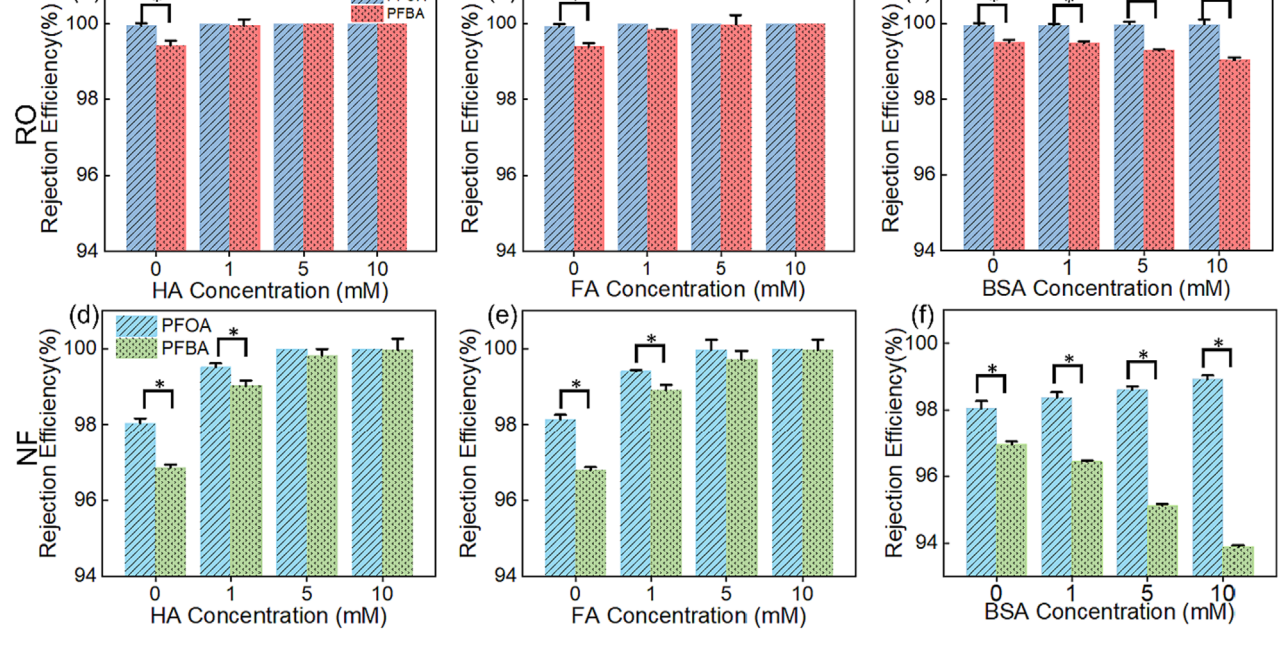
On the contrary, some studies reported that high NaCl concentrations (0.05-0.1 M) could induce a shielding effect on the negatively charged membrane and decrease the electrical double layer thickness, which reduces electrostatic repulsion between the membrane and PFAS and thus the rejection rate (Liu et al., 2022). We measured the surface zeta potential of RO and NF membrane under different ionic strengths. Compared with the pristine RO and NF membrane, the surface zeta potential significantly decreased with the increase of the cationic ion concentration as shown in Table S3. Our results show that when the NaCl concentration increased from 0 to 1000 mM, the permeate flux on RO membrane or NF membrane slightly decreased by 0.3% and 2.7%, respectively. Consequently, the PFOA/PFBA rejection decreased (especially evident for the NF membrane) as shown in Figure 4b-d. Compared with PFBA, the PFOA rejection was always higher at a given ionic strength, due to the difference in their molecular size and electrostatic forces between the membrane and the short-chain PFBA or the long-chain PFOA. The short-chain PFBA could penetrate the RO or NF membranes relatively more efficiently than the long-chain PFOA. Soriano et al. reported similar findings that the commercial NF and RO membranes had reduced removal for perfluorohexanoic acid (PFHxA) at 100 mg·L⁻¹ from industrial wastewater when the ionic strength was high (600 mg·L⁻¹) (Soriano et al., 2019). Clearly, the charge-shielding effect from cations may not be significant when the feed pH is lower than the isoelectric point of the membrane that may turn into positively charged (Lee et al., 2022). When the NaCl ionic strengths of feed solutions increased from 0 to 1000 mM, the permeate flux RO membrane decreased

due to increasing osmotic pressure, and the PFOA/PFBA rejection slightly decreased as shown in Figure 4. Compared with PFBA, PFOA rejection was thus higher at a given ionic strength. This may be attributed to the difference in the size and electrostatic forces between the short-chain **PFBA** and the long-chain The shorter-chain PFBA is easier to penetrate the RO/NF membrane under the weak electrostatic repulsion and weak size exclusion mechanism.

Moreover, membrane pores are likely to shrink under relatively high ionic strength (MgCl₂ and CaCl₂) and thus will enhance the size exclusion effect (Zhao et al., 2013, 2016). Conversely, some studies report that membrane pores may swell at excessive ionic strength and decrease the PFAS rejection (Xiong et al., 2021). To verify the membrane pore size change under high ionic strength, we evaluated the average pore size of the NF 90 membrane before and after a 24-h filtration test with different NaCl concentrations. The estimated pore radii are consistent for the different organic reference solutions (e.g., erythritol, xylose, and dextrose) as summarized in Table S3. The pristine NF 90 membrane has an average pore radius of 0.45 ± 0.07 nm, which is consistent to other reports (Košutić et al., 2007; Li et al., 2021; Nghiem & Hawkes, 2007). The used membrane had increased pore radius of 0.64 ± 0.06 nm, indicating that filtration of 1000-mM NaCl solution could affect the a polyamide network and the nanoporous structure.

Effect of organic matter

Natural organic matter (NOM), abundantly present in natural waters, can affect pollutant rejection due to membrane fouling or damages (Das & Ronen, 2022). Moreover, the membrane surface coverage by NOM could change the surface hydrophobicity and roughness, which may influence PFAS adsorption and rejection. The membrane fouling reduces the permeate flux and usually increases the PFAS rejection. Zhao et al., found that humic acid (HA) from 5 to 20 mg·L⁻¹ improved the PFOS rejection from 94.10% to 95.10% as the surface adsorption of HA increased the negative charges on the membrane surface, thereafter, enhancing the electrostatic exclusion of PFAS (Zhao et al., 2016). Wang et al. reported that PFOS adsorbed strongly on NOM via hydrophobic interactions, and as a result, both PFOS and organic matters were removed by NF with an increased PFOS rejection rate from 90% (without NOM) to 93% and 95% when bovine serum albumin (BSA) and sodium alginate (SA) were present in water (Wang et al., 2018). However, the PFBS rejection slightly decreased from 49% (without NOM) to 46% in the presence of BSA. Therefore,



Rejection efficiencies of perfluorooctanoic acid (PFOA) and perfluorobutanoic acid (PFBA) by the reverse osmosis (RO) and nanofiltration (NF) membranes with different concentration NOM. (a-d) With humic acid (HA); (b-e) with fluvic acid (FA); (c-f) with bovine serum albumin (BSA). * represent significant differences (p < 0.05, t test) between PFOA and PFBA test group.

the influence of NOM on PFAS may depend on specific PFAS species and the type of NOM, which are not well addressed.

Our results in Figure 5a,b show that, in comparison with PFOA/PFBA in DI water, HA and FA both lowered the concentrations of PFOA and PFBA in permeate from RO with removal rates of over 99.9%. Similarly, the presence of HA and FA also improved the PFOA and PFBA rejection efficiency on NF (Figure 5d,e). When the concentrations of HA and FA were higher than 1 mM, both PFOA and PFBA had increased removal rates of over 99.8%. HA seems to promote the removal of PFAS more significantly than FA due to the larger size of HA that results in the formation of larger molecular complexes or clusters with PFOA or PFBA. This larger complex contributes to an enhanced rejection efficiency of PFASs. Moreover, HA or FA will form a fouling layer to increase or decrease the electrostatic repulsion against PFAS. In Figure S5, the RO and NF membranes exhibited greater negative surface zeta potentials at low pH after HA and FA deposition. The HA-covered membrane also shows higher negative surface zeta potentials compared with that with FA. Thus, the electrostatic repulsion against PFAS should be more pronounced on HA-covered RO or NF membrane.

Besides the organic acids as the NOM surrogates, our study also evaluated the effect of protein-based organic matters that are also widely reported to cause filtration

membrane fouling. Figure 5c,f shows that with the increasing BSA concentration (1 to 10 mM), the permeate fluxes on the RO or NF membranes decreased due to membrane fouling, and the PFOA rejection efficiency slightly increased. However, the PFBA rejection efficiency decreased quite appreciably, which suggests the rejection mechanisms for PFOA and PFBA are different on RO or NF membranes. The long-chain PFOA is more excluded by the reduced pore channels after fouling. However, the rejection of PFBA is not likely to be affected by the pore size changes or configuration with BSA. Instead, the interaction between BSA and PFBA is suspected to reduce the back-diffusion of PFBA and thus increase the chance of PFBA's penetration (Zhao & Wang, 2016). Moreover, due to the surface adsorption or capture by the foulant layer, a foulant-enhanced CP may become significant and lead to reduced PFBA rejection.

Carbon chain length

The different PFAS structures such as carbon chain length, charge density, and end groups could vary their interactions with RO or NF membranes and porous transport, leading to different interplay of rejection or removal mechanisms (e.g., size exclusion, solution-diffusion, adsorption, or repulsion) (Boo et al., 2018). For most ionic and nonionic organic pollutants (e.g., pharmaceuticals

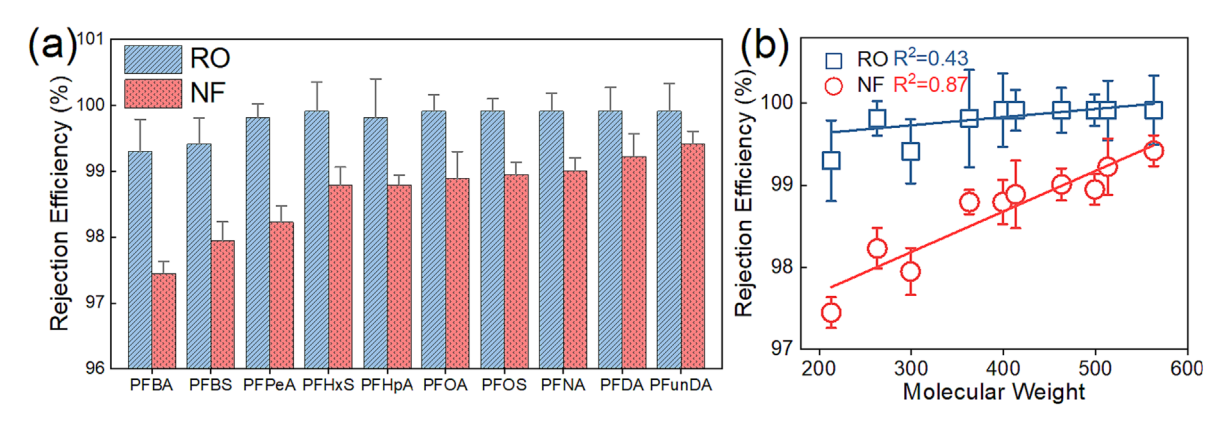


FIGURE 6 Rejection of 10 different perfluoroalkyl and polyfluoroalkyl substances (PFASs) with initial concentration of 10,000 ppb by the reverse osmosis (RO) and nanofiltration (NF) membranes under a transmembrane pressure of 55.16 bar for RO and 13.79 bar for NF in distilled (DI) water at a feed flow rate of 30 mL·min⁻¹ and room temperature for a filtration time of 24 h. (b) Relationship between PFAS molecular weight (MW) and their rejection by NF or RO membrane.

and personal care products, certain pesticides, disinfection by-products, and endocrine-disrupting compounds), the rejection rates increase as the molecular weight of the pollutant increases. Accordingly, the rejection efficiencies for PFPeA and PFBA were lower than other long-chain PFAS during NF filtration (Steinle-Darling Reinhard, 2008). Our results in Figure 6 compare the rejection of 10 different PFAS consisting of perfluorinated backbones ranging from 4 to 11 carbons (e.g., PFBA, PFpeA, PFHpA, PFOA, PFNA, PFDA, PFUnDA, PFBS, PFHxS, and PFOS). The rejection rate for the RO membrane is typically greater than 99%, while those for the NF membrane are from 97% to 99%. There is a rough correlation between the molecular weight of PFAS and rejection rates as shown in the inset, which shows that the rejection rates on RO or NF both increase with the molecular weight. The curve fit equations could also be employed to predict the rejection of PFAS at this specific operation conditions on the tested RO or NF. Clearly, more rigorous experiments are required to establish a robust database of PFAS rejection on different membranes with different pore sizes and surface properties as well as different operational conditions (e.g., transmembrane pressures and water matrixes or temperatures).

Analysis of PFAS rejection mechanisms by **RO/NF** membranes

PCA is an unsupervised clustering method that groups samples in a score plot based on the similarities between samples (e.g., the PFAS rejection data under various experimental conditions). One of the goals of PCA is to streamline the interconnections of different factors and

their contributions and weights on PFAS rejection. For example, when the solution pH changes, both the membrane surface zeta potential and the speciation of PFAS could vary, contributing to the variation in PFAS rejection. Figure 7 shows that the two principal components, PC1 and PC2, account for 32.0% and 28.0% of variance for the NF data, which represents up to 60% of the total variance. Similarly, the two major PCs for the RO data, PC1 and PC2, account for 48.0% and 25.0% of variance, which represents up to 73% of the total variance. Thus, the two PC1 and PC2 could reflect most of the information of all original variables (e.g., membrane pore size, pH, and PFAS concentration). The PCA plot shows the loadings (arrows) and scores (dots) of the experimental data. An arrow with a greater projected length on the axis of PC1 or PC2 indicates that the variable has a large loading and a strong relationship to PC1 or PC2. The dots represent data points taken from conditions.

For the PFAS rejection on RO membranes, the solution pH has a large positive loading along the direction of PC1 and membrane zeta potential has large negative loadings along the direction of PC1. In other words, the increase of pH value or the decrease of the membrane zeta potential may promote the PFAS rejection rate because of the enhanced electrostatic exclusion as mentioned above. This is supported by the observation that the membrane zeta potential decreased with an increase in the feed solution pH value. Moreover, the variable of feed concentration has a large negative loading on the PC2, indicating a negative correlation. This suggests that the feed concentration has a minor impact on PFAS rejection efficiency during RO filtration.

The PCA plot for the NF membranes shows very different interdependence of different variables from the observations for RO membranes. MW and ionic strength

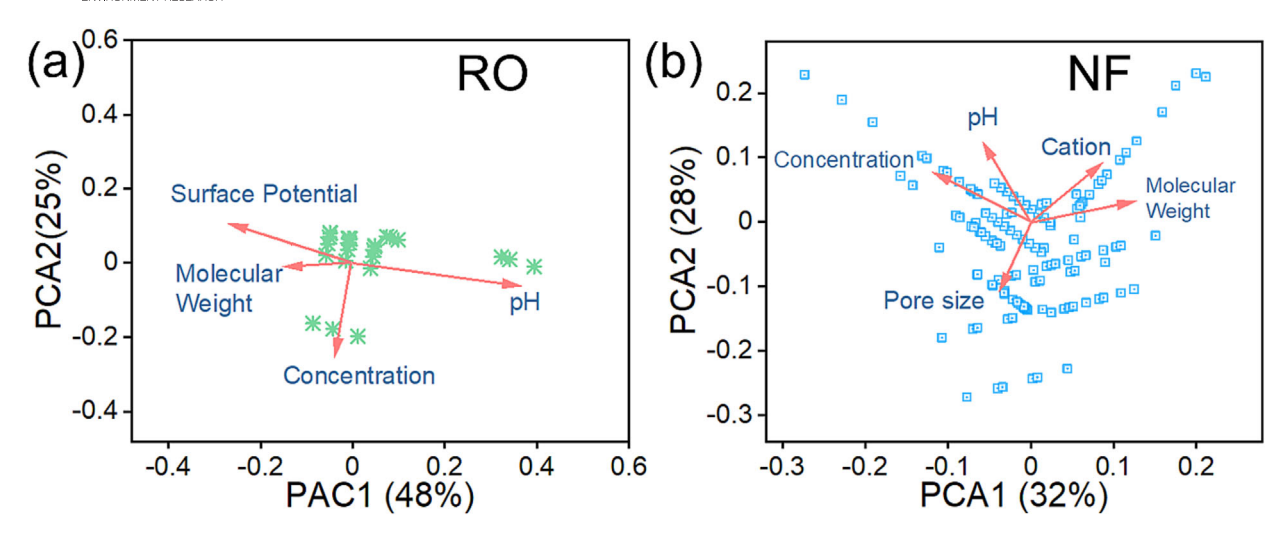


FIGURE 7 Principal component analysis (PCA) data of the intrinsic factors (perfluoroalkyl and polyfluoroalkyl substance [PFAS] molecular weight, membrane pore size) and extrinsic factors (pH value, initial concentration, cation concentration) for the PFAS rejection by the reverse osmosis (RO)/reverse osmosis (NF) membranes.

have a large positive loading on the PC1, whereas the variables of feeding PFAS concentration has large negative loadings on the PC1, which indicates that the variables of PFAS MW and ionic strength are positively correlated with PFAS rejection rate and negatively correlated with the variable of feeding PFAS concentration. Moreover, the variable of membrane pore size has a large negative loading on the PC2, whereas the variable of feeding pH value has a large positive loading on the PC2, which indicates that the variable of membrane pore size is positively correlated with PC2 and negatively correlated with the variable of feeding pH value. These correlations align with experimental observations, indicating that increasing the pH value or using an NF membrane with a smaller pore size enhances PFAS rejection. These findings are consistent with the results presented in Section 3.3.

CONCLUSION

The membrane separation and abatement of PFAS contamination in water is the most effective means compared with many other processes (e.g., adsorption) with the observed rejection efficiencies of over 99% for most RO membranes and 90%–99% for NF membranes. For the membrane rejection mechanisms, size exclusion, especially for those long carbon chain PFAS (>6 carbon), is another dominant rejection mechanism. Our results demonstrate the membrane rejection of 10 different molecular weights of PFAS. Increasing the transmembrane pressure could linearly increase the permeate flux and also the rejection of PFAS with a reduced level of the

PFOA/PFBA concentration in the permeate, suggesting that high-pressure RO operations could potentially increase both the permeate or water recovery and the PFAS rejection or removal. However, after the transmembrane pressure exceeded 41.37 bar, the permeate flux did not linearly increase but leveled off near 100 $L \cdot m^{-2} \cdot h^{-1}$, due to the evident compression effect on pore size or water transfer channels that was experimentally shown to reduce under ultra-high operational pressures. In addition to size exclusion, electrostatic interactions play an inevitably critical role for PFAS rejection. The surface zeta potentials for RO and NF membranes are generally negatively charged (-20 to -30 mV) at neutral pHs. Likewise, PFAS are anionic and, as a result, experience strong electrostatic repulsion against the membrane surface, as one of the key contributions to PFAS removal. For example, the pH variations change the surface zeta potential of the membranes. Decreasing the feed pH from 10 to 4 consistently reduced the PFOA/PFBA rejection for both the RO and NF membranes. However, the pH dependence of the PFAS rejection on RO was not as sensitive as on NF. Similar to pH, ionic strength affects the membrane properties and PFAS rejection, which largely depends on ionic types (monovalent, divalent, and trivalent). For instance, Ca²⁺ and Al³⁺ could interact with PFAS, leading to an increase in molecular cluster size and, consequently, an improvement in membrane rejection. SO_4^{2-} and PO_4^{3-} could strongly inhibit PFAS for the adsorption and membrane passage and rejection. Finally, the PCA data indicate that the major mechanism of PFAS rejection by NF is pore size or PFAS molecular weight and major mechanism of PFAS rejection by RO is electrostatic repulsion.



AUTHOR CONTRIBUTIONS

Qingquan Ma: Writing—original draft; investigation; review and editing; visualization; formal analysis; software. Qian Lei: Writing-original draft; review and editing. Fangzhou Liu: Writing-original draft; data curation; investigation. Zimu Song: Data curation; formal analysis. Boris Khusid: Funding acquisition; review and editing; resources; supervision; project administration. Wen Zhang: Conceptualization; funding acquisition; review and editing; project administration; resources; supervision.

ACKNOWLEDGMENTS

The authors gratefully acknowledge support for this research from National Science Foundation (NSF) Award IIP 1822130. This research was carried out in the NSF Industry/University Cooperative Research Center for Membrane Science, Engineering and Technology that has been supported by the NSF Award IIP-1822130. The authors want to thank the constructive feedback from the project mentors Uwe Beuscher from W.L. Gore & Associates, Inc., and Albert Wu from 3M as well as the support from the MAST center's Industrial Advisory Board (IAB) members.

CONFLICT OF INTEREST STATEMENT

The authors declare that they have no conflict of Interest.

DATA AVAILABILITY STATEMENT

The data that support the findings of this study are available from the corresponding author upon reasonable request.

ORCID

Qingquan Ma https://orcid.org/0000-0001-6879-6410 *Qian Lei* https://orcid.org/0000-0001-8455-8105 Fangzhou Liu https://orcid.org/0000-0003-0835-3399 Zimu Song https://orcid.org/0009-0001-7150-2345 Boris Khusid https://orcid.org/0000-0002-8604-1051 Wen Zhang https://orcid.org/0000-0001-8413-0598

REFERENCES

- Ang, W. S., & Elimelech, M. (2007). Protein (BSA) fouling of reverse osmosis membranes: Implications for wastewater reclamation. Journal of Membrane Science, 296(1-2), 83-92. https://doi.org/ 10.1016/j.memsci.2007.03.018
- Banks, D., Jun, B.-M., Heo, J., Her, N., Park, C. M., & Yoon, Y. (2020). Selected advanced water treatment technologies for perfluoroalkyl and polyfluoroalkyl substances: A review. Separation and Purification Technology, 231, 115929. https://doi.org/ 10.1016/j.seppur.2019.115929
- Bao, Y., Cagnetta, G., Huang, J., & Yu, G. (2020). Degradation of hexafluoropropylene oxide oligomer acids as PFOA alternatives in simulated nanofiltration concentrate: Effect of molecular

- structure. Chemical Engineering Journal, 382, 122866. https:// doi.org/10.1016/j.cej.2019.122866
- Baudequin, C., Mai, Z., Rakib, M., Deguerry, I., Severac, R., Pabon, M., & Couallier, E. (2014). Removal of fluorinated surfactants by reverse osmosis-Role of surfactants in membrane fouling. Journal of Membrane Science, 458, 111-119. https://doi. org/10.1016/j.memsci.2014.01.063
- Boo, C., Wang, Y., Zucker, I., Choo, Y., Osuji, C. O., & Elimelech, M. (2018). High performance nanofiltration membrane for effective removal of perfluoroalkyl substances at high water recovery. Environmental Science & Technology, 52(13), 7279-7288. https://doi.org/10.1021/acs.est.8b01040
- Boonya-Atichart, A., Boontanon, S. K., & Boontanon, N. (2016). Removal of perfluorooctanoic acid (PFOA) in groundwater by nanofiltration membrane. Water Science and Technology, 74(11), 2627-2633. https://doi.org/10.2166/wst.2016.434
- Boonya-atichart, A., Boontanon, S. K., & Boontanon, N. (2018). Study of hybrid membrane filtration and photocatalysis for removal of perfluorooctanoic acid (PFOA) in groundwater. Water Science and Technology, 2017(2), 561-569. https://doi. org/10.2166/wst.2018.178
- Brusseau, M. L., Anderson, R. H., & Guo, B. (2020). PFAS concentrations in soils: Background levels versus contaminated sites. Science of the Total Environment, 740, 140017. https://doi.org/ 10.1016/j.scitotenv.2020.140017
- Chen, X., Vanangamudi, A., Wang, J., Jegatheesan, J., Mishra, V., Sharma, R., Gray, S. R., Kujawa, J., Kujawski, W., & Wicaksana, F. (2020). Direct contact membrane distillation for effective concentration of perfluoroalkyl substances—Impact of surface fouling and material stability. Water Research, 182, 116010. https://doi.org/10.1016/j.watres.2020.116010
- Cummings, L.; Nelson, N.; Sickels, F.; Storms, C., Recommendation on perfluorinated compound treatment options for drinking water. New Jersey Drinking Water Quality Institute. 2015.
- D'Ambro, E. L., Pye, H. O., Bash, J. O., Bowyer, J., Allen, C., Efstathiou, C., Gilliam, R. C., Reynolds, L., Talgo, K., & Murphy, B. N. (2021). Characterizing the air emissions, transport, and deposition of per-and polyfluoroalkyl substances from a fluoropolymer manufacturing facility. Environmental Science & Technology, 55(2), 862-870. https://doi.org/10.1021/acs.est.0c06580
- Das, S., & Ronen, A. (2022). A review on removal and destruction of per-and polyfluoroalkyl substances (PFAS) by novel membranes. Membranes, 12(7), 662. https://doi.org/10.3390/ membranes12070662
- Davenport, D. M., Ritt, C. L., Verbeke, R., Dickmann, M., Egger, W., Vankelecom, I. F., & Elimelech, M. (2020). Thin film composite membrane compaction in high-pressure reverse osmosis. Journal of Membrane Science, 610, 118268. https://doi. org/10.1016/j.memsci.2020.118268
- Espana, V. A. A., Mallavarapu, M., & Naidu, R. (2015). Treatment technologies for aqueous perfluorooctanesulfonate (PFOS) and perfluorooctanoate (PFOA): A critical review with an emphasis on field testing. Environmental Technology and Innovation, 4, 168-181. https://doi.org/10.1016/j.eti.2015.06.001
- Fernandez, J. F., Jastorff, B., Stormann, R., Stolte, S., & Thoming, J. (2011). Thinking in terms of structure-activity-relationships (T-SAR): A tool to better understand nanofiltration membranes. Membranes (Basel), 1(3), 162-183. https://doi.org/10. 3390/membranes1030162



- Flores, C., Ventura, F., Martin-Alonso, J., & Caixach, J. (2013). Occurrence of perfluorooctane sulfonate (PFOS) and perfluorooctanoate (PFOA) in NE Spanish surface waters and their removal in a drinking water treatment plant that combines conventional and advanced treatments in parallel lines. Science of the Total Environment, 461, 618-626.
- Franke, V., Ullberg, M., McCleaf, P., Wålinder, M., Köhler, S. J., & Ahrens, L. (2021). The price of really clean water: Combining nanofiltration with granular activated carbon and anion exchange resins for the removal of per-and polyfluoralkyl substances (PFASs) in drinking water production. ACS ES&T Water, 1(4), 782-795. https://doi.org/10.1021/acsestwater. 0c00141
- Gagliano, E., Sgroi, M., Falciglia, P. P., Vagliasindi, F. G., & Roccaro, P. (2020). Removal of poly-and perfluoroalkyl substances (PFAS) from water by adsorption: Role of PFAS chain length, effect of organic matter and challenges in adsorbent regeneration. Water Research, 171, 115381. https://doi.org/10. 1016/j.watres.2019.115381
- Gu, Y.; Dong, W.; Wang, H., Degradation of perfluorooctane sulfonate (PFOS) by nanofiltration membrane enrichment-VUV/sulfite reduction. 2017. DEStech Transactions on Environment, Energy and Earth Sciences 2017 (ICSEEP).
- Hang, X., Chen, X., Luo, J., Cao, W., & Wan, Y. (2015). Removal and recovery of perfluorooctanoate from wastewater by nanofiltration. Separation and Purification Technology, 145, 120-129. https://doi.org/10.1016/j.seppur.2015.03.013
- Hu, X. C., Andrews, D. Q., Lindstrom, A. B., Bruton, T. A., Schaider, L. A., Grandjean, P., Lohmann, R., Carignan, C. C., Blum, A., & Balan, S. A. (2016). Detection of poly-and perfluoroalkyl substances (PFASs) in US drinking water linked to industrial sites, military fire training areas, and wastewater treatment plants. Environmental Science & Technology Letters, 3(10), 344–350. https://doi.org/10.1021/acs.estlett.6b00260
- Konradt, N., Kuhlen, J. G., Rohns, H.-P., Schmitt, B., Fischer, U., Binder, T., Schumacher, V., Wagner, C., Kamphausen, S., & Müller, U. (2021). Removal of trace organic contaminants by parallel operation of reverse osmosis and granular activated carbon for drinking water treatment. Membranes, 11(1), 33. https://doi.org/10.3390/membranes11010033
- Košutić, K., Dolar, D., Ašperger, D., & Kunst, B. (2007). Removal of antibiotics from a model wastewater by RO/NF membranes. Separation and Purification Technology, 53(3), 244–249. https:// doi.org/10.1016/j.seppur.2006.07.015
- Lee, T., Speth, T. F., & Nadagouda, M. N. (2022). High-pressure membrane filtration processes for separation of per-and polyfluoroalkyl substances (PFAS). Chemical Engineering Journal, 431, 134023. https://doi.org/10.1016/j.cej.2021.134023
- Li, M., Sun, F., Shang, W., Zhang, X., Dong, W., Dong, Z., & Zhao, S. (2021). Removal mechanisms of perfluorinated compounds (PFCs) by nanofiltration: Roles of membranecontaminant interactions. Chemical Engineering Journal, 406, 126814. https://doi.org/10.1016/j.cej.2020.126814
- Liu, C., Shen, Y., Zhao, X., Chen, Z., Gao, R., Zuo, Q., He, Q., Ma, J., & Zhi, Y. (2023). Removal of per-and polyfluoroalkyl substances by nanofiltration: Effect of molecular structure and coexisting natural organic matter. Journal of Hazardous Materials, 454, 131438. https://doi.org/10.1016/j.jhazmat.2023.131438

- Liu, C. J., Strathmann, T. J., & Bellona, C. (2021). Rejection of perand polyfluoroalkyl substances (PFASs) in aqueous filmforming foam by high-pressure membranes. Water Research, 188, 116546. https://doi.org/10.1016/j.watres.2020.116546
- Liu, Y.-L., & Sun, M. (2021). Ion exchange removal and resin regeneration to treat per-and polyfluoroalkyl ether acids and other emerging PFAS in drinking water. Water Research, 207, 117781. https://doi.org/10.1016/j.watres.2021.117781
- Liu, C., Zhao, X., Faria, A. F., Quiñones, K. Y. D., Zhang, C., He, Q., Ma, J., Shen, Y., & Zhi, Y. (2022). Evaluating the efficiency of nanofiltration and reverse osmosis membrane processes for the removal of per-and polyfluoroalkyl substances from water: A critical review. Separation and Purification Technology, 302, 122161. https://doi.org/10.1016/j.seppur.2022. 122161
- Luo, O., Liu, Y., Liu, G., & Zhao, C. (2016). Preparation, characterization and performance of poly (m-phenylene isophthalamide)/organically modified montmorillonite nanocomposite membranes in removal of perfluorooctane sulfonate. Journal of Environmental Sciences, 46, 126-133. https://doi.org/10.1016/j. jes.2015.10.032
- Ma, Q., Gao, J., Moussa, B., Young, J., Zhao, M., & Zhang, W. (2023). Electrosorption, desorption, and oxidation of perfluoroalkyl carboxylic acids (PFCAs) via MXene-based electrocatalytic membranes. ACS Applied Materials & Interfaces, 15, 29149-29159. https://doi.org/10.1021/acsami.3c03991
- Mastropietro, T. F., Bruno, R., Pardo, E., & Armentano, D. (2021). Reverse osmosis and nanofiltration membranes for highly efficient PFASs removal: Overview, challenges and future perspectives. Dalton Transactions, 50(16), 5398-5410. https://doi.org/ 10.1039/D1DT00360G
- Mouhoumed, E. I., Szymczyk, A., Schäfer, A., Paugam, L., & La, Y.-H. (2014). Physico-chemical characterization of polyamide NF/RO membranes: Insight from streaming current measurements. Journal of Membrane Science, 461, 130-138. https:// doi.org/10.1016/j.memsci.2014.03.025
- Nghiem, L. D., & Hawkes, S. (2007). Effects of membrane fouling on the nanofiltration of pharmaceutically active compounds (PhACs): Mechanisms and role of membrane pore size. Separation and Purification Technology, 57(1), 176-184. https://doi. org/10.1016/j.seppur.2007.04.002
- Nghiem, L. D., Schäfer, A. I., & Elimelech, M. (2004). Removal of natural hormones by nanofiltration membranes: Measurement, modeling, and mechanisms. Environmental Science & Technology, 38(6), 1888-1896. https://doi.org/10.1021/es034952r
- Rahman, M. F., Peldszus, S., & Anderson, W. B. (2014). Behaviour and fate of perfluoroalkyl and polyfluoroalkyl substances (PFASs) in drinking water treatment: A review. Water Research, 50, 318-340. https://doi.org/10.1016/j.watres.2013.10.045
- Rodowa, A. E., Knappe, D. R., Chiang, S.-Y. D., Pohlmann, D., Varley, C., Bodour, A., & Field, J. A. (2020). Pilot scale removal of per-and polyfluoroalkyl substances and precursors from AFFF-impacted groundwater by granular activated carbon. Environmental Science: Water Research & Technology, 6(4), 1083-1094. https://doi.org/10.1039/C9EW00936A
- Ross, I., McDonough, J., Miles, J., Storch, P., Thelakkat Kochunarayanan, P., Kalve, E., Hurst, J., Dasgupta, S. S., & Burdick, J. (2018). A review of emerging technologies for



- remediation of PFASs. Remediation Journal, 28(2), 101-126. https://doi.org/10.1002/rem.21553
- Senevirathna, S., Tanaka, S., Fujii, S., Kunacheva, C., Harada, H., Ariyadasa, B., & Shivakoti, B. (2010). Adsorption of perfluorooctane sulfonate (n-PFOS) onto non ion-exchange polymers and granular activated carbon: Batch and column test. Desalination, 260(1-3), 29-33. https://doi.org/10.1016/j.desal.2010. 05.005
- Shih, K., & Wang, F. (2013). Adsorption behavior of perfluorochemicals (PFCs) on boehmite: Influence of solution chemistry. Procedia Environmental Sciences, 18, 106-113. https://doi.org/10. 1016/j.proenv.2013.04.015
- Somrani, A., Shabani, M., Mohamed, Z., Ghaffour, N., Seibel, F., Briao, V. B., & Pontié, M. (2021). Transforming an end-of-life reverse osmosis membrane in a cationic exchange membrane and its application in a fungal microbial fuel cell. *Ionics*, 27(7), 3169-3184. https://doi.org/10.1007/s11581-021-04070-5
- Soriano, A., Gorri, D., & Urtiaga, A. (2019). Selection of high flux membrane for the effective removal of short-chain perfluorocarboxylic acids. Industrial & Engineering Chemistry Research, 58(8), 3329-3338. https://doi.org/10.1021/acs.iecr.8b05506
- Steinle-Darling, E., & Reinhard, M. (2008). Nanofiltration for trace organic contaminant removal: Structure, solution, and membrane fouling effects on the rejection of perfluorochemicals. Environmental Science & Technology, 42(14), 5292-5297. https://doi.org/10.1021/es703207s
- Tang, C. Y., Fu, Q. S., Robertson, A., Criddle, C. S., & Leckie, J. O. (2006). Use of reverse osmosis membranes to remove perfluorooctane sulfonate (PFOS) from semiconductor wastewater. Environmental Science & Technology, 40(23), 7343-7349. https://doi.org/10.1021/es060831q
- Wang, J., Wang, L., Xu, C., Zhi, R., Miao, R., Liang, T., Yue, X., Lv, Y., & Liu, T. (2018). Perfluorooctane sulfonate and perfluorobutane sulfonate removal from water by nanofiltration membrane: The roles of solute concentration, ionic strength, and macromolecular organic foulants. Chemical Engineering Journal, 332, 787-797. https://doi.org/10.1016/j.cej.2017.09.061
- Woodard, S., Berry, J., & Newman, B. (2017). Ion exchange resin for PFAS removal and pilot test comparison to GAC. Remediation Journal, 27(3), 19-27. https://doi.org/10.1002/rem.21515
- Xiong, J., Hou, Y., Wang, J., Liu, Z., Qu, Y., Li, Z., & Wang, X. (2021). The rejection of perfluoroalkyl substances by nanofiltration and reverse osmosis: Influencing factors and combination processes. Environmental Science: Water Research & Technology, 7(11), 1928-1943.
- Yadav, S., Ibrar, I., Al-Juboori, R. A., Singh, L., Ganbat, N., Kazwini, T., Karbassiyazdi, E., Samal, A. K., Subbiah, S., & Altaee, A. (2022). Updated review on emerging technologies for PFAS contaminated water treatment. Chemical Engineering Research and Design, 182, 667-700. https://doi.org/10.1016/j. cherd.2022.04.009

- Zhang, D., Zhang, W., & Liang, Y. (2019). Adsorption of perfluoroalkyl and polyfluoroalkyl substances (PFASs) from aqueous solution—A review. Science of the Total Environment, 694, 133606. https://doi.org/10.1016/j.scitotenv.2019.133606
- Zhao, C., Hu, G., Hou, D., Yu, L., Zhao, Y., Wang, J., Cao, A., & Zhai, Y. (2018). Study on the effects of cations and anions on the removal of perfluorooctane sulphonate by nanofiltration membrane. Separation and Purification Technology, 202, 385-396. https://doi.org/10.1016/j.seppur.2018.03.046
- Zhao, C., Tang, C. Y., Li, P., Adrian, P., & Hu, G. (2016). Perfluorooctane sulfonate removal by nanofiltration membrane-The effect and interaction of magnesium ion/humic acid. Journal of Membrane Science, 503, 31-41. https://doi.org/10.1016/j. memsci.2015.12.049
- Zhao, C., & Wang, W. (2016). Efficient faulty variable selection and parsimonious reconstruction modelling for fault isolation. Journal of Process Control, 38, 31-41. https://doi.org/10.1016/j. jprocont.2015.12.002
- Zhao, C., Zhang, J., He, G., Wang, T., Hou, D., & Luan, Z. (2013). Perfluorooctane sulfonate removal by nanofiltration membrane the role of calcium ions. Chemical Engineering Journal, 233, 224-232. https://doi.org/10.1016/j.cej.2013.08.027
- Zhi, Y., & Liu, J. (2015). Adsorption of perfluoroalkyl acids by carbonaceous adsorbents: Effect of carbon surface chemistry. Environmental Pollution, 202, 168-176. https://doi.org/10.1016/j. envpol.2015.03.019
- Zhi, Y., Zhao, X., Qian, S., Faria, A. F., Lu, X., Wang, X., Li, W., Han, L., Tao, Z., & He, Q. (2022). Removing emerging perfluoroalkyl ether acids and fluorotelomer sulfonates from water by nanofiltration membranes: Insights into performance and underlying mechanisms. Separation and Purification Technology, 298, 121648. https://doi.org/10.1016/j.seppur.2022.121648

SUPPORTING INFORMATION

Additional supporting information can be found online in the Supporting Information section at the end of this article.

How to cite this article: Ma, Q., Lei, Q., Liu, F., Song, Z., Khusid, B., & Zhang, W. (2024). Evaluation of commercial nanofiltration and reverse osmosis membrane filtration to remove per-and polyfluoroalkyl substances (PFAS): Effects of transmembrane pressures and water matrices. Water Environment Research, 96(2), e10983. https://doi.org/10.1002/wer.10983